Long-term evolution of corrected NOAA/MEPED energetic proton fluxes and their relation to geomagnetic indices

Timo Asikainen*, Kalevi Mursula

Department of Physics, Centre of Excellence in Research, PO Box 3000, University of Oulu, FIN-90014, Finland

ABSTRACT

We study the relationship between energetic 120–250 keV proton fluxes and geomagnetic Ap, AE, Dxt indices using the recently corrected measurements of the MEPED instrument onboard the low-altitude NOAA/POES satellites. Corrected database spans from 1979 to present, and allows us to reliably study the long-term variation of energetic proton fluxes over several solar cycles. Contrary to uncorrected fluxes, which can be more than an order of magnitude too low, the corrected fluxes display a systematic solar cycle variation closely resembling the variation of Ap and AE indices with a maximum in the declining solar cycle phase and a minimum in solar minimum. We also find that trapped fluxes are enhanced relative to precipitating fluxes in the declining phases and solar minima. This supports the fact that high-speed solar wind streams are the most significant driver of energetic proton fluxes. We compute the correlations between fluxes and indices in a range of time scales, and show that they are significantly improved by the flux correction. We find that precipitating fluxes correlate better than trapped fluxes with Ap/AE indices at all time scales, and the highest correlation is found with Ap. For precipitating fluxes these correlations depend weakly on time scale, but for trapped fluxes the correlation significantly increases from daily scale to solar rotation and longer time scales. Comparing the fluxes to Dxt index shows a complex relationship, where the fluxes depend not only on Dxt value but also on its time derivative.

© 2014 Elsevier Ltd. All rights reserved.

1. Introduction

The relationship between magnetospheric energetic particles (tens of keV to MeV energy) and geomagnetic indices is an outstanding question which has been studied extensively. Already soon after the first satellite measurements in the 1960s it was discovered that particle precipitation often occurs simultaneously with substorms recorded by ground-based magnetometers (e.g., DeForest and McIlwain, 1971). Many studies have shown a clear correlation with geomagnetic AE/AL indices and the intensity of auroral particle precipitation (tens of eV to few tens of keV energy), assuming a linear relation between AE index and the energy input of precipitating particles into the upper atmosphere (e.g., Akasofu, 1981). Recent studies have suggested a more complicated, nonlinear relationship (see, e.g. Østgaard et al., 2002, who studied 100 eV–100 keV electrons). Many studies have also compared auroral particle precipitation with geomagnetic Kp and Ap indices which describe overall geomagnetic activity at mid-latitudes (e.g., Hardy et al., 1985,

1987, 1989). They have demonstrated that the intensity of auroral precipitation increases with increasing geomagnetic activity.

The relationship between higher energy particles with energies from several tens of keV to thousands of keV and geomagnetic activity indices has also been studied widely. Relativistic electrons of a few MeV energy and their relationship to Kp index have been extensively studied due to their importance for space weather (e.g., Nagai, 1988; Baker et al., 1989, 1990). Several studies have demonstrated that the behaviour of relativistic electron fluxes at geosynchronous orbit is rather complicated, with the fluxes often peaking a few days after an enhancement in solar wind speed and in the Kp index (e.g., Friedel et al., 2002; Lyatsky and Khazanov, 2008; Reeves et al., 2011, and references therein) probably after subsequent acceleration by ULF waves (Elkington et al., 1999) and/or VLF waves like whistler-mode chorus (e.g., Horne and Thorne, 2003, and references therein). Despite these complications a rough long-term correlation between the Kp index and the relativistic electron fluxes does exist. Recently Rodger et al. (2010) studied the relativistic electron precipitation observed by the low-altitude and geostationary NOAA satellites. They demonstrated that enhancements in the daily fluxes of low-altitude and geosynchronous relativistic electrons and Kp index display a similar temporal evolution.

* Corresponding author.
E-mail address: timo.asikainen@oulu.fi (T. Asikainen).

The long-term relationship between energetic protons and ions in the ring current and the geomagnetic indices has also been studied, although it has received less attention recently than relativistic electrons. Baker et al. (1979) studied protons of few hundred keV energy and showed that their enhancements at geosynchronous orbit closely correlate with enhancements in the Kp index. More recently Søraas et al. (2002, 2005) studied the relationship between the Dst index and energetic protons measured at low-altitude orbit by the NOAA/POES satellites. They showed that the temporal evolution of the Dst index could be quite accurately modelled by using the observed energetic proton fluxes as a source term for the model ring current, implying that the protons observed by the low-altitude satellites measure primarily the injections into the ring current rather than the ring current intensity.

In this paper we consider the long-term relationship between energetic proton fluxes and several common geomagnetic indices by using particle measurements of the low-altitude NOAA/POES satellites that have operated nearly continuously since 1979. The major complication with the NOAA proton data has been the degradation of the energetic proton detectors of the MEPED instrument onboard these satellites caused by radiation damage. This leads to severely underestimated fluxes and artificial long-term trends in the uncorrected data (Galand and Evans, 2000; McFadden, 2007; Asikainen and Mursula, 2011; Asikainen et al., 2012). We have recently corrected the entire NOAA/MEPED proton database of all satellites for radiation damage and other instrumental problems (Asikainen and Mursula, 2011; Asikainen et al., 2012), and produced a systematically calibrated dataset that spans over three solar cycles. Using this corrected database we study here the relationship between the proton fluxes and the geomagnetic Ap, AE and Dxt (an extended and recalculated version of Dst index, Karinen and Mursula, 2005) indices. Our motivation is to see how well these commonly used geomagnetic indices can describe long-term variations in the intensity of energetic proton populations. Comparison with indices also allows us to quantitatively demonstrate the improvement brought by the correction of the MEPED proton fluxes. The contents of the paper are organized as follows. Section 2 describes the basic properties of NOAA/POES satellites, the MEPED instrument and correction of the proton data. In Section 3 we discuss the overall solar cycle variation of the fluxes and indices, demonstrating the differences between the uncorrected and corrected proton fluxes. In Section 4 we study the correlations between the proton fluxes and geomagnetic indices, and show that they are significantly improved by the correction of the fluxes. The conclusions are given in the last section.

2. Data

In this work we use the energetic proton measurements by the NOAA/POES satellites, which fly on nearly circular, polar orbits with a nominal altitude of about 850 km and an orbital period of about 102 min. The orbital planes relative to the Sun–Earth line stay relatively constant (Sun synchronous), although over several years the orbital planes typically rotate slightly. The NOAA/POES satellites occupy three types of orbits with different orientations (dawn–dusk, noon–midnight, pre-noon–pre-midnight). To obtain a homogeneous dataset we selected for the present study only those satellites (NOAA-06, NOAA-08, NOAA-10, NOAA-12 and NOAA-15) that are on a dawn–dusk orbit since they form the longest and most uniform series of measurements since 1979.

The NOAA/POES satellites include a SEM (Space Environment Monitor) instrument package for measuring energetic protons and electrons. The satellites up to NOAA-14 had the SEM-1 version of the instrument package while from NOAA-15 onwards the satellites carry an improved version called SEM-2. The MEPED (Medium Energy

Proton Electron Detector) instrument, which is a part of SEM, consists of two separate sub-instruments that measure energetic protons and electrons. The energetic protons are measured at the nominal energy range from 30 keV upwards. In the SEM-1 instruments the proton fluxes were measured in five energy channels and in the SEM-2 version in six energy channels. MEPED measures particles by two nearly orthogonal telescopes. The 0° telescope in SEM-1 points radially outward from Earth. In SEM-2 the 0° telescope has further been rotated from the radial direction by 9° clockwise around the spacecraft velocity vector to ensure clear field of view. The 90° telescope in SEM-1 points roughly perpendicular to the spacecraft orbital plane while in SEM-2 it points roughly antiparallel to the spacecraft velocity vector. Accordingly the 0° telescopes in SEM-1 and SEM-2 point roughly in the same direction and are thus comparable, but the 90° telescopes point in different directions, leading to systematic differences between SEM-1 and SEM-2. The measured count rates (particles/s) are converted to physical fluxes (particles/cm^2 sr s) by dividing with the nominal geometric factor which is $G=0.0095$ cm^2 sr for SEM-1 and $G=0.01$ cm^2 sr for SEM-2. (A more detailed description of SEM-1 is given by Hill et al., 2005; Seale and Bushnell, 1987; Raben et al., 1995 while SEM-2 is described by Evans and Greer, 2000.)

The MEPED proton detectors have been observed to degrade over time due to radiation damage, which leads to underestimated fluxes and artificial long-term trends in the uncorrected data (Galand and Evans, 2000; McFadden, 2007; Asikainen and Mursula, 2011; Asikainen et al., 2012). Recently we conducted a quantitative analysis of the effect of radiation damage on the MEPED proton detectors and presented a new method to recalibrate the fluxes of all NOAA/POES satellites (Asikainen and Mursula, 2011). We showed that, typically, the data in the beginning of the operational period of a new satellite is fairly reliable, but already after a few years the radiation damage has degraded the instruments so badly that the data can no longer be trusted without recalibration. Radiation damage effectively increases the instrument energy thresholds from their nominal values by a factor which increases in time and depends on the cumulative radiation dose imposed on the instrument. Due to this effect the count rates measured by the MEPED instruments do not correspond to their nominal energies. In addition to degradation due to the radiation damage we recently showed that the back detectors of NOAA-12 0° and NOAA-08 90° telescopes also suffer from increased electronic noise (Asikainen et al., 2012). The back detector measures the highest energy particles that pass though the front detector, which measures lower energy protons. Increased electronic noise in the back detector produces false counts that erase a portion of real counts from the front detector (due to anti-coincidence logics between front and back detectors). This also decreases the measured count rates in the lower energy channels measured by the front detector. We have studied and corrected also this electronic noise problem in the corrected count rates (Asikainen et al., 2012).

The estimated effective energy thresholds (Asikainen et al., 2012) can be used to calculate the proton fluxes at their correct energy ranges. This is done by fitting a polynomial interpolant to the measured integral spectra in log–log scale and computing the fluxes at the desired energies by using this interpolant (Asikainen and Mursula, 2011). This method produces reliable results for fluxes above the lowest effective energy. In this study we use this method to calculate the proton fluxes in the 120–250 keV energy range for the 0° and 90° telescopes of all dawn–dusk satellites. The lower bound of 120 keV is defined by the largest effective energy threshold of the lowest energy channel (Asikainen et al., 2012). The fluxes were first computed using 16 s averaged data (eight 2 s measurements), whereafter daily averages were calculated using the data only from the northern hemisphere and L-shells above $L=2$. The energetic
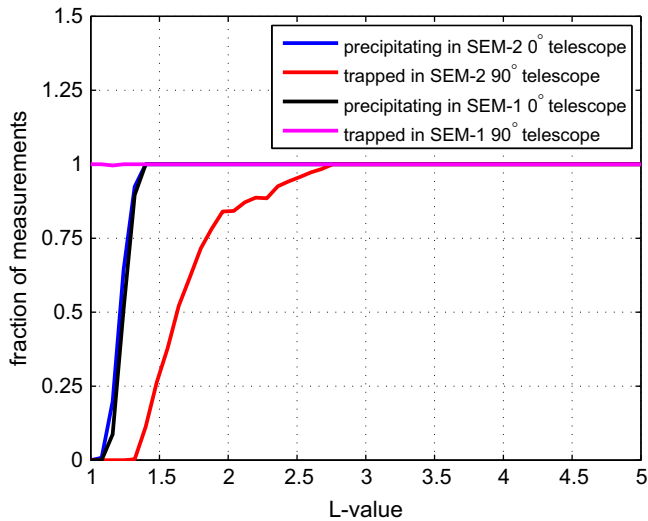
Fig. 1. Fraction of measurements that correspond to precipitating particles in the 0° telescope and locally trapped particles in the 90° telescope separately for SEM-1 and SEM-2 instruments.

particle fluxes in the low-altitude NOAA/POES orbit are strongly dependent on the intensity of local geomagnetic field. This leads to significant diurnal variation in the fluxes sampled by each NOAA/POES satellite. We use daily averages of fluxes in order to smooth out the diurnal variation and to have a better comparison of the global fluxes with global geomagnetic indices, which also use longitudinally averaged measurements. Selecting the L-shells above $L=2$ avoids the high fluxes of relativistic electrons present in the South Atlantic Anomaly region, which extend even to the northern hemisphere at the low L-shells. Relativistic electrons can be a problem for the MEPED proton measurements since they occasionally contaminate some of the proton energy channels. This contamination is most severe in the highest energy proton channel (P5 in SEM-1 and P6 in SEM-2) but some contamination may also occur at the lowest energy channels (P1–P3). At $L > 2$ the fluxes of relativistic electrons are typically over an order of magnitude lower than those of 120–250 keV protons. Furthermore the geometric factor for relativistic electrons is over an order of magnitude smaller than for protons in P1–P3 channels (see Yando et al., 2011). Thus, for the selected L region, relativistic electron contamination is not a significant problem. Since the telescope pitch angles change along the satellite orbit, we performed a statistical analysis of MEPED pitch angles to estimate the fraction of measurements at different L-shells, which correspond to precipitating particles in the 0° telescopes and trapped particles in 90° telescopes. This was done by comparing the pitch angle of the telescope's center of view with the local bounce loss cone angle. The results of this pitch angle analysis are shown in Fig. 1 for SEM-1 and SEM-2 separately. We found that in the selected L-region of $L > 2$ the SEM-1 and SEM-2 MEPED 0° telescopes always measure particles that are in the local bounce loss cone, i.e., precipitating. In SEM-1 the 90° telescope always measures locally trapped particles. In SEM-2 at $L > 2$ over 84% of the 90° telescope measurements correspond to locally trapped particles. (Note, however, that most of the locally trapped particles measured by the NOAA satellites are typically in the drift loss cone.) Based on this analysis the $L=2$ limit is also convenient for determining average precipitating and trapped fluxes from the two telescopes.

In addition to NOAA/POES data we also use geomagnetic Ap and AE indices and the Dxt index, which is a version of the Dst index, which is extended backwards in time to 1932 and corrects some of the known errors of Dst, e.g., the erroneous latitude

normalization of individual stations contributing to the index and erroneously determined Sq variation and overall level of the index a few individual years (Karinen and Mursula, 2005). The latest version of the Dxt index was obtained from the online Dcx/Dxt index server maintained at the University of Oulu, http://dcx.oulu.fi. In this study our data spans from 7 July 1979 to 10 November 2012.

3. Solar cycle variation of energetic protons and geomagnetic indices

Fig. 2 shows the time series of 30-day averaged energetic proton fluxes in the energy range 120–250 keV from the two directional telescopes. In addition to the proton fluxes, Fig. 2 also shows the geomagnetic Ap, AE and Dxt indices as well as the solar wind pressure corrected Dxt, the Dxt* index (Asikainen et al., 2010). Comparison of the corrected and uncorrected fluxes shows the dramatic effect of the correction. As pointed out earlier (Asikainen et al., 2012), the uncorrected data severely underestimates the fluxes. They also display an excessively large solar cycle variation because NOAA-06, NOAA-12 and NOAA-15 were all launched near solar cycle maximum (NOAA-06 in 1979, NOAA-12 in 1991 and NOAA-15 in 1998) and started degrading in the declining phase of the solar cycle. Degradation of the instruments led to erroneously large flux decrease from solar maximum to the next solar minimum. This is clearly seen as a steep decrease in the uncorrected flux level from 1982 to 1986, from 1992 to 1997, and from 2001 to 2009.

The solar cycle variation in the corrected data is much smaller than in the uncorrected data especially for the 0° telescope. The strongest fluxes are attained either in the early (1982, 1991, 2003) or in the later declining phase (1986, 1994, 2004–2005). Other, weaker, enhancements are seen during sunspot maxima (e.g., 1989 and 2000). The smallest fluxes are typically seen during solar cycle minima and especially during the unusually deep solar minimum in 2009. The unique character of the solar cycle minimum in 2009 has been seen in several solar/heliospheric parameters and geomagnetic activity indices (e.g., Russell et al., 2010; Tsurutani et al., 2011; Clette and Lefévre, 2012). Fig. 2 verifies the uniquely low level of corrected fluxes of energetic protons during this minimum. It is also interesting to note how sharply the fluxes increase after the minimum in 2010 at the beginning of solar cycle 24. In fact, only in a few months the proton fluxes increase back to the level previously attained a few years earlier.

The solar cycle variation in the 90° telescope is quite similar to that in the 0° telescope, but there are some differences in the relative amplitudes of the flux enhancements. For example, the difference in the two flux peaks in 1991 and 1994 is smaller in the 90° telescope than in the 0° telescope. On the other hand, the two peaks in 1982 and 1986 are more similar in magnitude in the 0° telescope than they are in the 90° telescope. Note that since the 90° telescopes in SEM-1 and SEM-2 instruments have a different orientation (SEM-2 measures slightly smaller pitch angles than SEM-1, see Section 2), there may be a systematic difference in the 90° flux levels before and after 1 July 1998 when NOAA-15, the first SEM-2 satellite, started producing data.

In order to study whether such difference exists, Fig. 3 shows the 30-day averages of the ratio of daily corrected (red) and uncorrected (blue) 90° and 0° fluxes. The 90°/0° ratio is generally larger than one because in the considered L-shells the 90° telescope measures protons at larger pitch angles than the 0° telescope, and the trapped population is typically larger than the precipitating. The correction has the largest effect on the 90°/0° ratio in 1994–1998. The particularly large differences between the corrected and uncorrected ratios in 1997–1998 result from the severe degradation of NOAA-12 0° data due to increased back detector noise (Asikainen et al., 2012). Note that most of the time
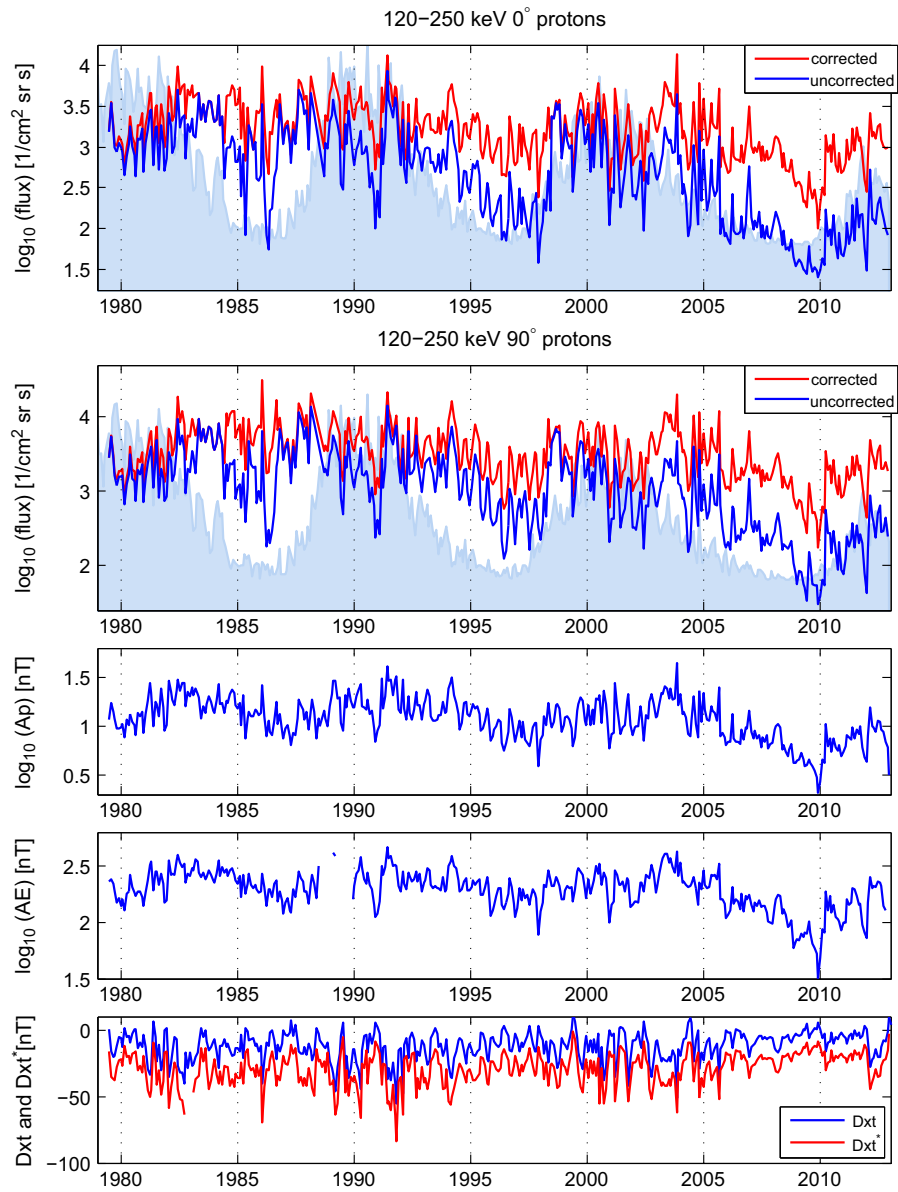
Fig. 2. The two top panels show the 30-day averaged 0° and 90° protons from 120–250 keV energy range. The red (blue) curve shows the time series of corrected (uncorrected) fluxes. The light shading in the background shows the sunspot cycle. The two middle panels show the 30-day averaged Ap and AE indices. The bottom panel shows the 30-day averaged Dxt index (blue curve) and the solar wind pressure corrected Dxt* (red curve). (For interpretation of the references to colour in this figure caption, the reader is referred to the web version of this paper.)
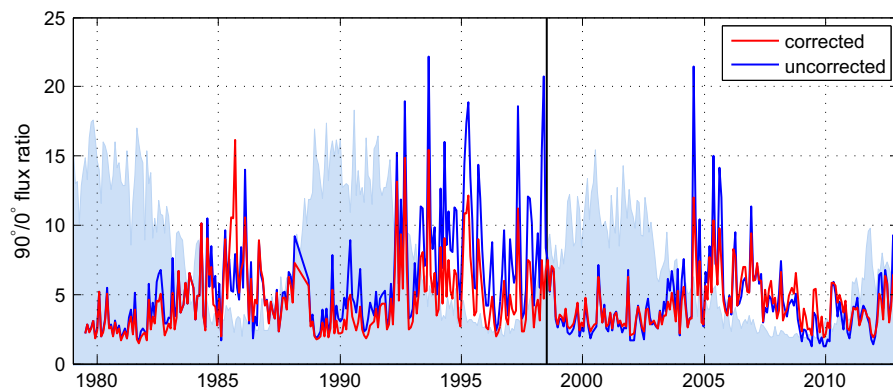
Fig. 3. 30-day averages of the ratio of daily 90° and 0° corrected (red) and uncorrected (blue) proton fluxes in 120–250 keV energy range. The black vertical line at 1 July 1998 indicates the launch of NOAA-15 and separates the eras of SEM-1 and SEM-2 measurements. (For interpretation of the references to colour in this figure caption, the reader is referred to the web version of this paper.)

the uncorrected 90°/0° flux ratio is larger than the corrected one. As pointed out by Asikainen et al. (2012), the 90° telescopes typically suffer greater radiation damage than the 0°, but the energy spectrum is typically harder in the 90° telescope than in the 0° telescope. When calculating the corrected fluxes this leads to a greater relative increase of the fluxes in the 0° telescope than in the 90° telescope, and consequently to smaller 90°/0° flux ratio in the corrected fluxes in comparison to the uncorrected ones. The 90°/0° ratio also shows a significant solar cycle variation, which peaks in the late declining phase and attains a minimum around solar maximum. This behaviour most likely arises due to alternating domination of high-speed streams (HSS) during the declining phase and CMEs during solar maxima. It is likely that HSS's produce more long-lasting populations of trapped energetic protons than CME storms, which produce strong ring current proton populations that decay relatively fast. The faster decay in CME storms partly results from the trapped populations being at relatively lower L-shells ($L \approx 3$), where the collisional losses of ring current ions are larger than at higher L-shells ($L \approx 5-6$) where the trapped populations are typically created during HSS storms. The faster decay during CME storms also partly results from strong flow-out losses in the early recovery phase (Kozyra and Liemohn, 2003). It is likely that these differences in the decay time of the trapped ion populations lead to the 90°/0° ratio being smaller during CME driven storms than during HSS driven storms. Comparing the SEM-1 and SEM-2 time series one cannot see a clear systematic difference between the corrected 90°/0° ratios of these two time periods. This is in agreement with the fact that even though SEM-1 and SEM-2 90° telescopes point in different directions, the pitch angles corresponding to their field-of-views are quite similar in the considered L-shell range ($L > 2$). Based on this we estimate that the overall systematic difference between the SEM-1 and SEM-2 90° fluxes is small and does not significantly affect the results of this paper.

The geomagnetic Ap and AE indices display a closely similar long-term variation with the proton fluxes (see Fig. 2). Most maxima in Ap and AE indices are seen during the declining phase (1982 and 1986, 1991 and 1994, 2003 and 2005), some in solar maximum years (1989 and 2000), in agreement with simultaneous maxima in corrected proton fluxes. The minima in these indices coincide with solar minima in 1987, 1997 and 2009. It is well known that both the overall geomagnetic activity (described by the Ap index) and especially the substorm activity (AE index) are driven predominantly by high speed solar wind streams and associated corotating interaction regions that maximize in the declining phase of the solar cycle (e.g., Tanskanen et al., 2005, 2011). During solar maxima the variations in the indices and fluxes are mainly due to geomagnetic storms driven by coronal mass ejections.

4. Correlation between proton fluxes and geomagnetic indices

Let us now discuss the correlation between the proton fluxes and geomagnetic indices. The correlation coefficient and corresponding 95% confidence limit between the logarithmic 30-day averaged corrected (uncorrected) 0° proton fluxes (depicted in Fig. 2) and Ap index is 0.932 ± 0.013 (0.85 ± 0.03), and between fluxes and the AE index 0.87 ± 0.03 (0.78 ± 0.05). For the 90° fluxes the corresponding correlation coefficient with the Ap index is 0.89 ± 0.02 (0.85 ± 0.03) and with the AE index 0.84 ± 0.04 (0.77 ± 0.05). These and other correlation coefficients discussed below have been gathered in Table 1. The results clearly show that correlations are greatly improved after correcting the fluxes. One can also see that the 0° fluxes especially for daily averages, correlate better with the indices than the 90° fluxes, which may partly reflect a true, closer similarity between the 0° fluxes of precipitating ions and geomagnetic indices and partly the greater homogeneity of the 0° fluxes. Note that this difference is only visible after the correction. Note also that the correlations are systematically better for the Ap index than AE, probably because Ap is a more global measure of geomagnetic activity than AE responding also to other current systems in space than only the auroral electrojets. We also computed the correlations between the fluxes and the AL index (not shown), which describes the westward auroral electrojet. However, we found that at short time scales up to a few days the correlation with AL is slightly smaller than with AE. At longer time scales the correlation with AL is slightly higher than with AE, but the difference is not statistically significant.

The long-term variation of the Dxt index in Fig. 2 is roughly similar to that of the Ap and AE indices. The largest Dxt decreases are observed at solar maxima (1989 and 2001) and in the declining phase (in 1982, 1986, 1991, 1994 and 2003). Note that while the overall solar cycle variation in the Dxt index resembles that of the Ap and AE indices, the relative amplitude of individual disturbances may be quite different in Dxt. The correlation coefficient between the logarithmic 30-day averaged corrected (uncorrected) 0° fluxes and logarithmic (absolute values of) Dxt index is 0.69 ± 0.06 (0.56 ± 0.08). The corresponding correlation coefficient between the 0° fluxes and Dxt* is 0.75 ± 0.05 (0.59 ± 0.07). For the 90° fluxes the correlation coefficient with Dxt is 0.68 ± 0.06 (0.59 ± 0.07) and with the Dxt* index 0.75 ± 0.05 (0.63 ± 0.07). (Note that when computing the correlation between logarithmic fluxes and logarithmic Dxt indices the positive Dxt/Dxt* values were discarded.) These results show that the correlations between the fluxes and the Dxt/Dxt* indices are significantly weaker than with the Ap/AE indices. One can also see a better correlation with the Dxt* index than with Dxt. Note that this physically motivated improvement becomes more clearly and systematically visible when using the corrected fluxes.

Table 1

Correlation coefficients and corresponding 95% confidence limits between 0° and 90° proton fluxes and geomagnetic Ap, AE, Dxt and Dxt* indices. The correlations are shown for 30-day averages and daily averages.

	0° corrected	0° uncorrected	90° corrected	90° uncorrected
30-day averages				
Ap	0.932 ± 0.013	0.85 ± 0.03	0.89 ± 0.02	0.85 ± 0.03
AE	0.87 ± 0.03	0.78 ± 0.05	0.84 ± 0.04	0.77 ± 0.05
Dxt	0.69 ± 0.06	0.56 ± 0.08	0.68 ± 0.06	0.59 ± 0.07
Dxt*	0.75 ± 0.05	0.59 ± 0.07	0.75 ± 0.05	0.63 ± 0.07
Daily averages				
Ap	0.922 ± 0.003	0.850 ± 0.005	0.819 ± 0.006	0.710 ± 0.009
AE	0.863 ± 0.005	0.803 ± 0.007	0.761 ± 0.008	0.647 ± 0.011
Dxt	0.609 ± 0.014	0.556 ± 0.015	0.621 ± 0.013	0.53 ± 0.02
Dxt*	0.685 ± 0.010	0.605 ± 0.012	0.718 ± 0.009	0.603 ± 0.012
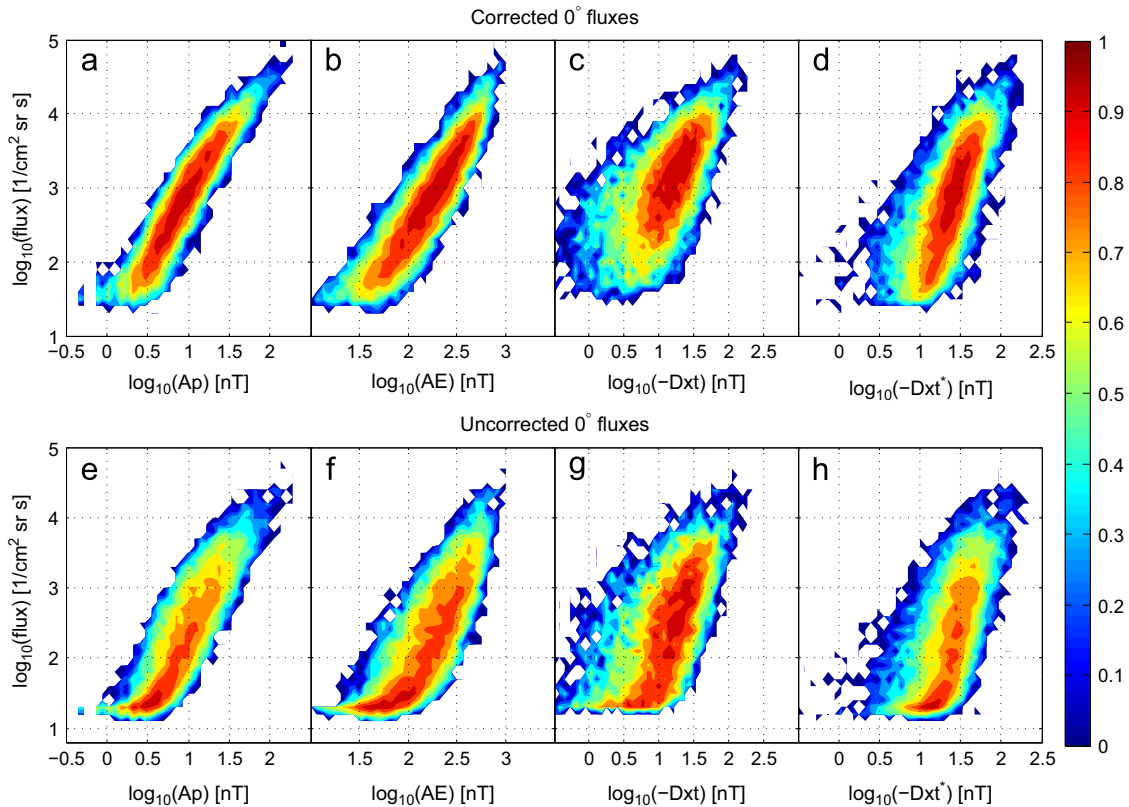
Fig. 4. The distribution of daily averaged corrected (top) and uncorrected (bottom) 0° proton fluxes in 120–250 keV energy range as a function of daily averaged Ap index (a and e), AE index (b and f), Dxt index (c and g) and pressure corrected Dxt* index (e and h). Color scale shows the normalized logarithmic density of data points in the figure. (For interpretation of the references to colour in this figure caption, the reader is referred to the web version of this paper.)

In order to study the relation between the fluxes and the indices in more detail we show in Fig. 4 the distribution of the corrected and uncorrected daily averaged 0° proton fluxes as a function of the four daily averaged geomagnetic indices. One can see a clear overall correlation between fluxes and all indices. However, the distributions of the uncorrected proton fluxes show much more scatter than those of the corrected fluxes and are strongly skewed at low flux values because the uncorrected fluxes are underestimated. The lowest limit of the fluxes is determined by the instrument background noise level (one-count level), which is roughly $\log_{10}(\text{flux}) = 1.1$ for the 16 s averaging time. Fluxes below the background level cannot be distinguished from noise, which is why the number of data points close to this level is increased as the underestimation of the fluxes becomes more severe. As shown in Table 1, the best correlation was found for the corrected 0° fluxes and the Ap index (cc=0.922 ± 0.003). Note that despite the skewed distribution, the uncorrected fluxes also display clear correlation with the indices above the noise level, and the best correlation for the uncorrected 0° fluxes is also obtained with the Ap index (cc=0.85 ± 0.03). For the corrected fluxes a somewhat lower, but still good correlation is found for the AE index (0.863 ± 0.005). Fig. 4 shows that although correlation with the daily Dxt index is statistically significant (cc=0.609 ± 0.014) the scatter is very large indicating that the Dxt (or Dst) index is not a very good measure for proton fluxes at low altitudes. This supports the earlier results, e.g., by Søraas et al. (2002), which indicate that the proton fluxes observed by NOAA/POES satellite are better related to ring current injections. The scatter in the fluxes is considerably reduced after correcting the Dxt index for solar wind pressure. Accordingly, the correlation between daily proton fluxes and the Dxt* index (cc=0.685 ± 0.010) is better than with the Dxt index suggesting that the magnetopause currents

(unrelated to the ring current particle content) contribute a large fraction to the Dxt index especially at small Dxt (quiet times), where the scatter is largest, as seen in Fig. 4.

The reason for the overall weaker correlation with Dxt in comparison to the other studied indices is most likely that the protons are brought to low altitudes by processes which scatter them towards the loss cone. These processes are enhanced during substorms, which inject energy into the ring current, and during ring current decay when particle precipitation from the ring current is enhanced, e.g., by wave–particle interactions. The energy injections are better included in Ap and AE indices than in the Dxt index, which mostly measures the absolute level of the ring current. A large difference between the MEPED proton fluxes and Dxt is due to the fact that a given value of Dxt can reflect very different magnetospheric conditions and levels of precipitation, depending on the phase of the storm (main phase vs. recovery phase). To see whether this is true we investigated the relationship between the two in more detail. In addition to comparing the proton fluxes to the Dxt index we compared them also to the daily sum of rectified positive and negative hourly Dxt differences, computed for each day by the equations

$$\Delta Dxt_{\text{pos}} = \sum_{i=1}^{23} \max(Dxt_{i+1} - Dxt_i, 0)$$

$$\Delta Dxt_{\text{neg}} = \sum_{i=1}^{23} \min(Dxt_{i+1} - Dxt_i, 0). \qquad (1)$$

Assuming the that hourly change in the Dxt index is an indication of the amount of particles lost from (positive change) or injected into (negative change) the ring current, the sum of positive Dxt differences is a rough measure for the total amount of particles lost from the ring current during a day. Similarly the sum
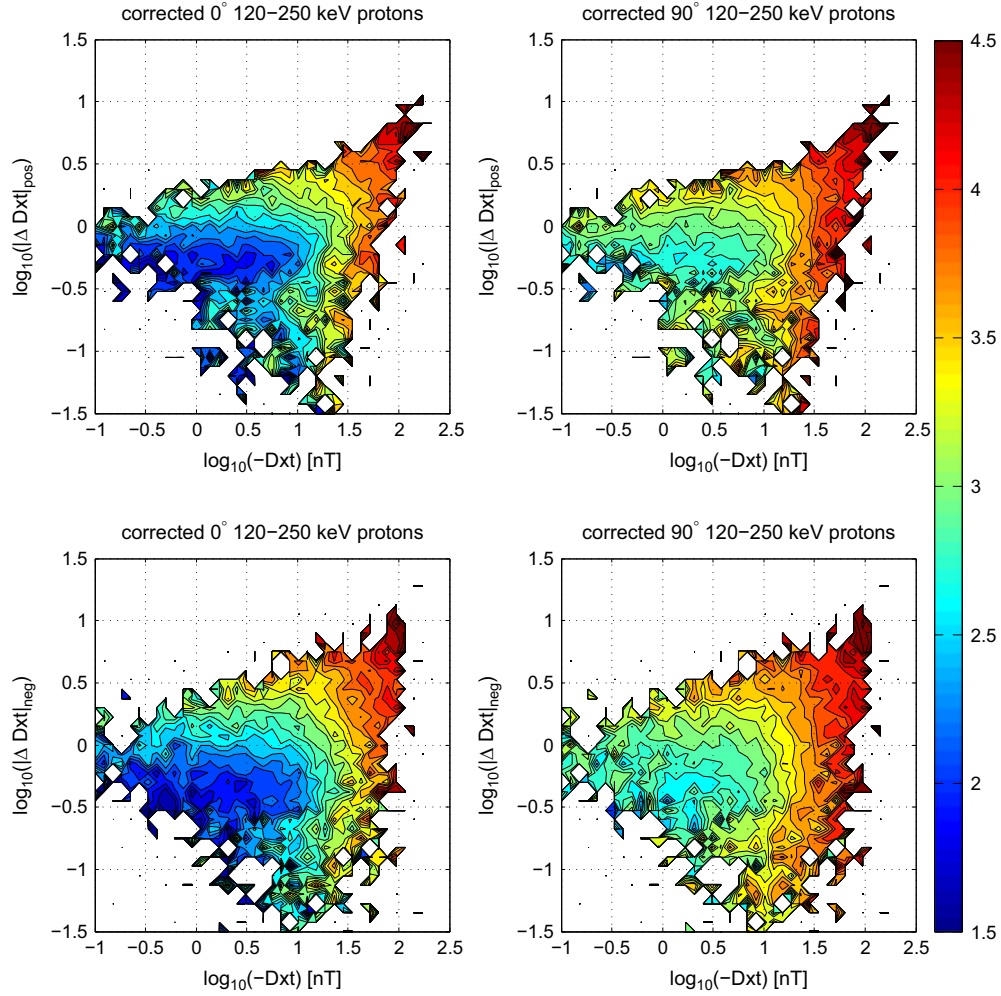
Fig. 5. The distribution of corrected 0° (left) and 90° (right) 120–250 keV protons as a function of Dxt index and the daily sum of rectified positive (top) and negative (bottom) hourly Dxt differences. The colour scale indicates the average flux. (For interpretation of the references to colour in this figure caption, the reader is referred to the web version of this paper.)

of negative Dxt differences roughly measures the total amount of particles injected into the ring current during a day. Fig. 5 shows the average corrected 0° and 90° fluxes as a function of Dxt index and the summed differences. For both telescopes one can see that the fluxes depend on both the Dxt and the summed Dxt differences. When the summed Dxt differences are small the fluxes seem to depend significantly only on the Dxt index. Conversely, when the Dxt magnitude is small the fluxes increase with the magnitude of the summed Dxt differences and show little dependence on the Dxt. When both, the Dxt index and the summed differences are large the fluxes generally depend on both of these parameters. These findings indicate a rather complex relationship between the energetic protons observed by the NOAA/POES satellites and the Dxt (Dst) index, and verify that the fluxes are evidently enhanced by both particle injections into the ring current and by ring current losses. In both of these cases particles from the ring current precipitate and are observed at low altitudes. On the other hand, in the absence of significant injections or losses a certain proportion of ring current protons is still observed at low altitudes as they bounce on the field lines.

As shown in Table 1, for daily and 30-day averages, the correlations between the fluxes and indices allow us to quantify the improvement in the proton fluxes brought by the correction. We will further improve on this by studying how the correlations change when considering a range of different time scales. Fig. 6

shows the correlation coefficients between the corrected and uncorrected 0° and 90° proton fluxes and the four indices at time scales from 1 day to 1 year. It is obvious from Fig. 6 that the correction produces a clear and, for most time scales and indices, a statistically significant increase in correlation. The most significant improvements in correlation are observed for short time scales up to a few days. As the time scale increases, the number of correlated data points decreases and, consequently, the statistical significance of the improvement becomes smaller.

The corrected 0° fluxes with the Ap index show higher correlation at all time scales than any other flux-index pair. The correlation with Ap increases slightly up to a few days and then slightly drops attaining a small local minimum around 10 days. After that the correlation slightly increases with time scale until about half a year and then decreases slightly. (Note, however, that variations beyond 10 days are quite small and barely statistically significant). Correlation between 0° flux and AE index is somewhat smaller, but develops somewhat similarly with time scale, except that the correlation does not increase until after 10 days, when it is more systematic. Correlation with the Dxt index is much smaller at all time scales than with the Ap and AE indices. It depicts a varying local maximum between 10–30 days and a local minimum at about 60 days, and a rapid increase thereafter. Correlation with Dxt* index is better than with Dxt at all time scales and depicts a more systematic increase with time scale than for Dxt.
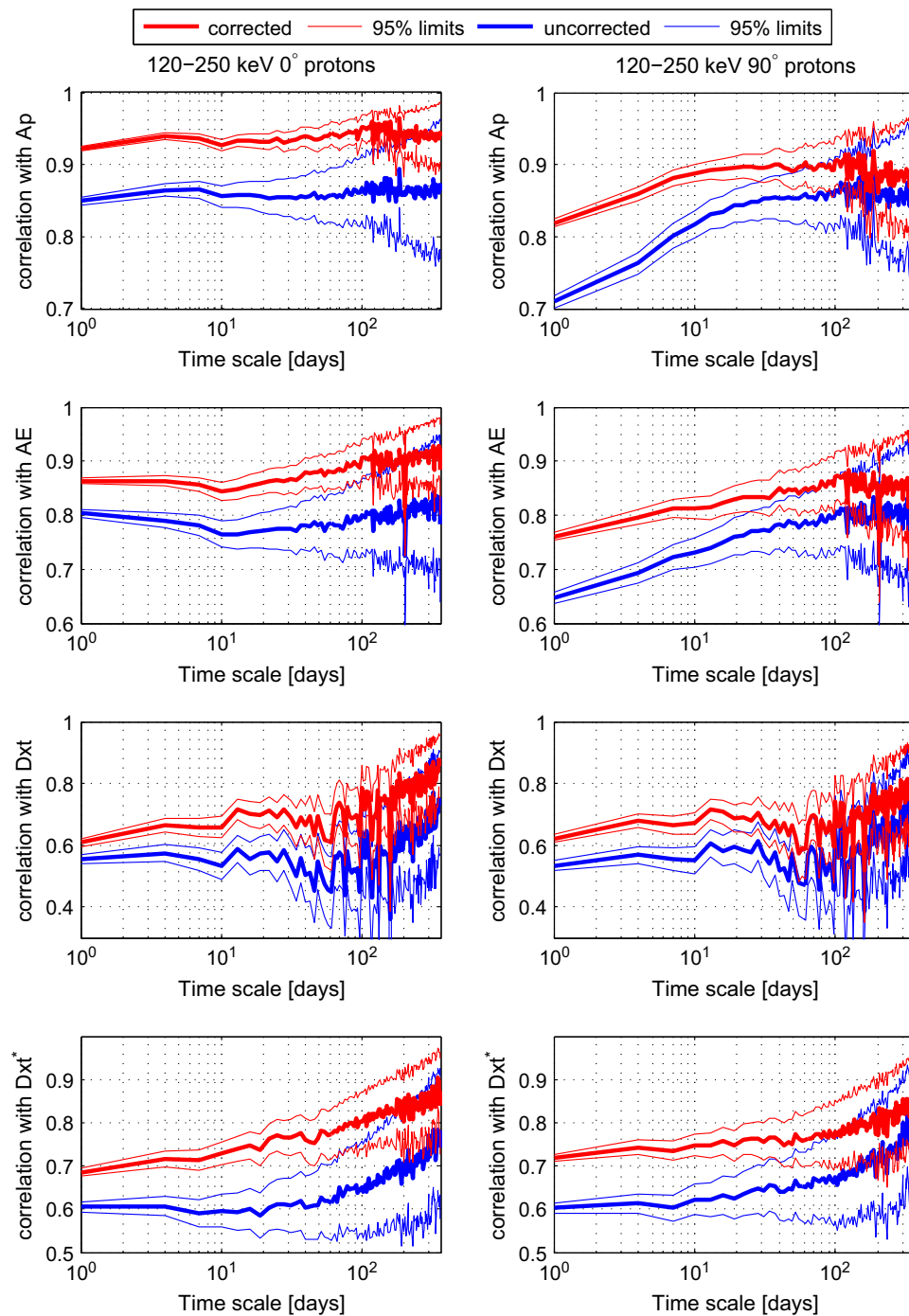
Fig. 6. Correlation coefficients between geomagnetic indices and the proton fluxes at different time scales. Left hand plots correspond to the $0°$ fluxes and the right hand plots to the $90°$ fluxes. Red curves depict corrected fluxes and blue curves the uncorrected fluxes. The thin lines indicate the 95% confidence limits for the correlation coefficients. (For interpretation of the references to colour in this figure caption, the reader is referred to the web version of this paper.)

The correlation coefficients between $90°$ fluxes and Ap/AE indices are generally smaller than those of $0°$ fluxes and behave differently as a function of time scale. The correlation with the Ap index rises rather steeply from 1 day up to about 10 days, and stays roughly constant until half a year. Correlation between $90°$ fluxes and the AE index increases rather systematically as a function of time scale until about half a year, decreasing slightly thereafter. This rather strong increase of correlation of $90°$ fluxes and Ap/AE indices with time scale most likely arises because time scales longer than ~ 10 days emphasize variations related to occurrence of storms (e.g., variation with solar rotation, seasonal variations and solar cycle variations). Time scales shorter than this emphasize

variations occurring within individual storms. The difference between $0°$ and $90°$ flux correlations at short time scales indicates that during individual storms the Ap/AE indices better depict variations in the precipitating fluxes ($0°$) than in the trapped fluxes ($90°$). At long (seasonal and solar cycle) time scales the temporal evolution of Ap/AE and both fluxes greatly resemble each other.

Contrary to Ap and AE indices, the correlations between the $90°$ fluxes and Dxt/Dxt* indices behave very similarly at all time scales as the $0°$ fluxes. Moreover, contrary to Ap and AE indices, the correlation with $0°$ fluxes is not generally larger than with $90°$ fluxes for Dxt/Dxt* indices. In fact the only statistically significant difference between $0°$ and $90°$ flux correlations with Dxt/Dxt*

indices is found at short time scales where the correlation with Dxt* is slightly (but statistically significantly) larger for the 90° fluxes than for the 0° fluxes. The slightly better correlation of 90° fluxes with Dxt/Dxt* compared to 0° fluxes at short time scales emphasizes the better correspondence of locally trapped fluxes with Dxt indices during individual storms.

5. Conclusions

In this paper we studied the relationship of energetic proton fluxes and geomagnetic indices using the recently corrected measurements of the MEPED instrument onboard the low-altitude NOAA/POES satellites. The entire NOAA/POES database spans over three solar cycles from 1979 to present and allows us to study the long-term variation of the proton fluxes reliably for the first time. We have shown earlier (Asikainen et al., 2012) that the uncorrected fluxes, which suffer from the effects of instrument degradation and detector noise, display an erroneous and inhomogeneous long-term evolution. Here it was shown that only the corrected energetic proton fluxes depict a correct solar cycle variation with the fluxes typically peaking in the declining phase of the solar cycle, with a secondary maximum often observed during the solar maximum, and the minimum fluxes typically observed at the solar minima. The solar cycle variation found in the corrected proton fluxes greatly resembles the variation of geomagnetic Ap and AE indices. Corrected fluxes raise the relative height of the peak in fall 2003 to one of the largest flux peaks (highest in 0° flux) during the three solar cycles, in a good agreement with the Ap/AE indices. We verified that the proton fluxes attained a uniquely low level during the last solar minimum in 2009, after which they rapidly increased in the beginning of solar cycle 24. The observed solar cycle variation suggests that the high-speed solar wind streams are the most significant driver of energetic proton fluxes in the magnetosphere. This interpretation is supported by the similar solar cycle behaviour of Ap/AE indices and the fluxes, and the fact that high speed streams explain the dominant fraction of geomagnetic activity (e.g., Richardson and Cane, 2012). We also found that the ratio of 90° and 0° fluxes (trapped/precipitating flux ratio) has a solar cycle variation, with the ratio peaking in the declining phase and solar minimum, and having a minimum at solar maximum. This systematic behaviour also reflects the different response of proton populations to high speed solar wind streams (dominant in the declining phase) and CMEs (dominant at solar maximum).

To quantify the improvement in the fluxes due to correction, and to study the connection between fluxes and the indices in more detail, we computed the correlation coefficients between the fluxes and geomagnetic Ap, AE, Dxt (corrected Dst index) and Dxt* (solar wind pressure corrected Dxt) indices at different time scales from 1 day to 1 year. We found that generally the correlation was best for Ap and slightly smaller for AE. The overall best correlation was found between 0° (precipitating) fluxes and the Ap index, which was above 0.92 at all time scales and larger than for any other flux-index pair. The smallest correlation was found for Dxt, while the correction for solar wind pressure improved the correlation with Dxt* significantly. This shows that the magnetopause currents unrelated to the energetic particle content of the ring current are a significant factor in the Dxt index. The higher correlation of proton fluxes with Ap and AE indices suggests that the fluxes observed by the low altitude satellites depend more closely on geomagnetic and substorm activity, which scatter protons towards the loss cone, than on the intensity of the ring current. The smaller correlation with the Dxt/Dxt* indices may result from the fact that a given Dxt/Dxt* value can be observed during very different times of magnetospheric activity (storm main phase and recovery phase). We found that while weak proton fluxes can depend either on the Dxt/Dxt* value or its time derivative separately, the highest fluxes depend on both of these factors. This further verifies that the low altitude proton fluxes do not only depend on the absolute level of the ring current but also its temporal change. Regarding the effect of the flux correction, we found that all correlations were improved by the correction, most of them by a statistically significant amount. This gives additional evidence for the validity of the correction and the necessity to use a reliable and homogeneous long-term dataset.

References

Akasofu, S.-I., 1981. Energy coupling between the solar wind and the magnetosphere. Space Sci. Rev. 28 (2), 121–190.

Asikainen, T., Mursula, K., 2011. Recalibration of NOAA/MEPED energetic proton measurements. J. Atmos. Solar Terr. Phys. 73, 335–347, http://dx.doi.org/10.1016/j.jastp.2009.12.011.

Asikainen, T., Maliniemi, V., Mursula, K., 2010. Modeling the contributions of ring, tail and magnetopause currents to the corrected Dst index. J. Geophys. Res. 115, A12203, http://dx.doi.org/10.1029/2010JA015774.

Asikainen, T., Mursula, K., Maliniemi, V., 2012. Correction of detector noise and recalibration of NOAA/MEPED energetic proton fluxes. J. Geophys. Res. 117, A09204, http://dx.doi.org/10.1029/2012JA017593.

Baker, D., Belian, R.D., Higbie, P.R., Hones Jr., E.W., 1979. High-energy magnetospheric protons and their dependence on geomagnetic and interplanetary conditions. J. Geophys. Res. 84 (A12) 7138–7154. http://dx.doi.org/10.1029/JA084iA12p07138.

Baker, D., Blake, J., Callis, L.B., Belian, R.D., Cayton, T.E., 1989. Relativistic electrons near geostationary orbit: evidence for internal magnetospheric acceleration. Geophys. Res. Lett. 16 (6), 559–562, http://dx.doi.org/10.1029/GL016i006p00559.

Baker, D., McPherron, R., Cayton, T., Klebesadel, R., 1990. Linear prediction filter analysis of relativistic electron properties at 6.6 RE. J. Geophys. Res. 95 (A9), 15133–15140, http://dx.doi.org/10.1029/JA095iA09p15133.

Clette, F., Lefévre, L., 2012. Are the sunspots really vanishing?—Anomalies in solar cycle 23 and implications for long-term models and proxies. J. Space Weather Space Clim. 2 (A06), 80–82, http://dx.doi.org/10.1051/swsc/2012007.

DeForest, S., McIlwain, C., 1971. Plasma clouds in the magnetosphere. J. Geophys. Res. 76 (16), 3587, http://dx.doi.org/10.1029/JA076i016p03587.

Elkington, S., Hudson, M., Chan, A., 1999. Acceleration of relativistic electrons via drift-resonance interaction with toroidal mode Pc5 ULF oscillations. Geophys. Res. Lett. 26, 3273.

Evans, D.S., Greer, M.S., Polar Orbiting Environmental Satellite Space Environment Monitor—2: Instrument Descriptions and Archive Data Documentation. NOAA Technical Memorandum, Boulder, Colorado OAR SEC-93.

Friedel, R., Reeves, G.D., Obara, T., 2002. Relativistic electron dynamics in the inner magnetosphere review. J. Atmos. Sol. Terr. Phys. 62 (2), 26582, http://dx.doi.org/10.1016/S1364–6826(01)00088–8.

Galand, M., Evans, D., Radiation Damage of the Proton MEPED Detector on POES (TIROS/NOAA) Satellites. NOAA Technical Memorandum, Boulder, Colorado OAR 456-SEC 42.

Hardy, D., Gussenhoven, M., Raistrick, R., 1985. A statistical model of auroral electron precipitation. J. Geophys. Res. 90 (A5), 4229–4248.

Hardy, D., Gussenhoven, M., Raistrick, R., 1987. Statistical and functional representations of pattern of auroral energy flux, number flux, and conductivity. J. Geophys. Res. 92 (A11), 12275–12294.

Hardy, D., Gussenhoven, M., Brautigam, D., 1989. A statistical model of auroral ion precipitation. J. Geophys. Res. 94 (A1), 370–392.

Hill, V.J., Evans, D.S., Sauer, H.H., TIROS-N/NOAA Satellites Space Environment Monitor archive Tape Documentation. NOAA Technical Memorandum, Boulder, Colorado ERL SEL-71.

Horne, R., Thorne, R., 2003. Relativistic electron acceleration and precipitation during resonant interactions with whistler-mode chorus. Geophys. Res. Lett. 30 (10), 1527, http://dx.doi.org/10.1029/2003GL016973.

Karinen, A., Mursula, K., 2005. A new reconstruction of the Dst index for 1932–2002. Ann. Geophys. 23, 475–485.

Kozyra, J., Liemohn, M., 2003. Ring current energy input and decay. Space Sci. Rev. 109, 105–131, http://dx.doi.org/10.5194/angeo–29–839–2011.

Lyatsky, W., Khazanov, G.V., 2008. Effect of geomagnetic disturbances and solar wind density on relativistic electrons at geostationary orbit. J. Geophys. Res. 113, A08224, http://dx.doi.org/10.1029/2008JA013048.

McFadden, J., Evans, D., Kasprzak, W., et al., 2007. In-Flight Instrument Calibration and Performance Verification. In: Wüest, M., Evans, D.S., von Steiger, R. (Ed.), Calibration of Particle Instruments in Space Physics. ISSI Scientific Report, ESA Publications Division, vol. SR-007, pp. 277–385.

Nagai, T., 1988. Space weather forecast: prediction of relativistic electron intensity at synchronous orbit. Geophys. Res. Lett. 15 (5), 425–428, http://dx.doi.org/10.1029/GL015i005p00425.

Østgaard, N., Vondrak, R., Gjerloev, J., Germany, G., 2002. A relation between the energy deposition by electron precipitation and geomagnetic indices during substorms. J. Geophys. Res. 107 (A9), 1246, http://dx.doi.org/10.1029/2001JA002003.

Raben, V.J., Evans, D.S., Sauer, H.H., Sahm, S.R., Huynh, M. TIROS/NOAA Satellite Space Environment Monitor Data Archive Documentation: 1995 update. NOAA Technical Memorandum, Boulder, Colorado ERL SEL-86.

Reeves, G., Morley, S., Friedel, R., Henderson, M., Cayton, T., Cunningham, G., Blake, J., Christensen, R., Thomsen, D., 2011. On the relationship between relativistic electron flux and solar wind velocity: Paulikas and Blake revisited. J. Geophys. Res. 116, A02213, http://dx.doi.org/10.1029/2010JA015735.

Richardson, I., Cane, H., 2012. Near-earth solar wind ows and related geomagnetic activity during more than four solar cycles (1963–2011). J. Space Weather Space Clim. 2 (A02). http://dx.doi.org/10.1029/2001JA000123.

Rodger, C., Clilverd, M., Green, J., Lam, M., 2010. Use of POES SEM-2 observations to examine radiation belt dynamics and energetic electron precipitation into the atmosphere. J. Geophys. Res. 115, A04202, http://dx.doi.org/10.1029/2008JA014023.

Russell, C., Luhmann, J., Jian, L., 2010. How unprecedented a solar minimum? Rev. Geophys. 48 (RG2004), http://dx.doi.org/10.1029/2009RG000316.

Seale, R.A., Bushnell, R.H., The TIROS-N/NOAA A-J Space Environment Monitor subsystem. NOAA Technical Memorandum, Boulder, Colorado ERL SEL-75.

Søraas, F., Aarsnes, K., Oksavik, K., 2002. Ring current intensity estimated from low-altitude proton observations. J. Geophys. Res. 107 (A7) http://dx.doi.org/10.1029/2001JA000123.

Søraas, F., Aarsnes, K., Carlsen, D.V., Oksavik, K., Evans, D.S., 2005. Ring current behavior as revealed by energetic proton precipitation. In: Pulkkinen, T., Tsyganenko, N., Friedel, R., (Eds.), The Inner Magnetosphere: Physics and Modeling, Geophysical Monograph. American Geophysical Union, vol. 155, pp. 237–248.

Tanskanen, E., Slavin, J., Tanskanen, A., Viljanen, A., Pulkkinen, T., Koskinen, H., Pulkkinen, A., Eastwood, J., 2005. Magnetospheric substorms are strongly modulated by interplanetary high-speed streams. Geophys. Res. Lett. 32, L16104, http://dx.doi.org/10.1029/2005GL023318.

Tanskanen, E., Pulkkinen, T., Viljanen, A., Mursula, K., Partamies, N., Slavin, J., 2011. From space weather towards space climate time scales: substorm analysis from 1993 to 2008. J. Geophys. Res. 116, A00I34, http://dx.doi.org/10.1029/2010JA015788.

Tsurutani, B.T., Echer, E., Gonzalez, W.D., 2011. The solar and interplanetary causes of the recent minimum in geomagnetic activity (MGA23): a combination of midlatitude small coronal holes, low IMF BZ variances, low solar wind speeds and low solar magnetic fields. Ann. Geophys. 29, 839–849, http://dx.doi.org/10.5194/angeo–29–839–2011.

Yando, K., Millan, R., Green, J., Evans, D., 2011. A Monte Carlo simulation of the NOAA POES medium energy proton and electron detector instrument. J. Geophys. Res. 116, A10231, http://dx.doi.org/10.1029/2011JA016671.